



CFD Analysis of the Flow around Simplified Next-Generation Train Subjected to Crosswinds at Low Yaw Angles

Mohammad Arafat^{1,*}, Izuan Amin Ishak¹

¹ Department of Mechanical Engineering Technology, Faculty of Engineering Technology, University Tun Hussein Onn Malaysia, Edu Hub Pagoh, 84600, Muar, Johor, Malaysia

ARTICLE INFO

Article history:

Received 31 December 2021

Received in revised form 13 February 2022

Accepted 14 February 2022

Available online 31 March 2022

Keywords:

Aerodynamic; CFD; Crosswinds; Next-generation Train (NGT); URANS

ABSTRACT

The development of Next-Generation Trains (NGT) made of lightweight materials is a challenging task for the transport industry. It reduces axle loads, which saves money by lowering rail track maintenance costs and the amount of energy needed to drive vehicles. However, the increasing speed and decreasing mass of high-speed trains, on the other hand, raises concerns about the effects of strong crosswinds on their aerodynamics and train stability. As a result, the purpose of this research is to investigate the unsteady flow structure around an NGT in crosswind using a Computational Fluid Dynamics (CFD) technique known as Unsteady Reynolds Averaged Navier-Stokes (URANS). Based on the height of the train model and the velocity, the Reynolds number for the simulation used was 1.3×10^6 . The simulation run in four different crosswind angles: 5°, 10°, 15°, and 20°. The simulation results were compared with experimental results. The findings revealed that a larger yaw angle, which is primarily determined by the incoming wind velocity, can lead to higher flow separation and a more complex three-dimensional flow around the train. Additionally, when the wind angle is small, separation of flow and wakes is limited to the train's end; however, as the wind angle increases, separation of flow occurs from the train's upper and lower corners, indicating that the vortices formed as a result of the flow passing over the roof top and underbody. Finally, the study's findings will contribute to a better understanding of the flow characteristics around an NGT in crosswinds, which is simply impossible to achieve through full-scale testing due to the cost, resources, and accuracy.

1. Introduction

In many countries around the world, high-speed trains are regarded as a quick, safe, and comfortable mode of transportation. High-speed rail would be far more efficient and cost-effective than air or automobile for trips of 100-1000 km, yielding significant cost, fuel, and time savings. Consequently, the demand for this mode of transportation has been increasing rapidly in recent years. Currently, the development of Next-Generation Trains (NGT) made of lightweight materials is a challenging issue for the train transportation industry. Lightweight trains minimize axle loads, which

* Corresponding author.

E-mail address: marafatbd@gmail.com (Mohammad Arafat)

saves money by lowering rail track maintenance costs and the energy required to drive vehicles [1, 2]. As a result, travel time can be significantly reduced, and the train can operate at optimum efficiency [3]. Aside from train weight, the aerodynamics of the train is a crucial consideration for engineers in designing NGT. Knowledge of unsteady flow structures and the associated acting forces on the surface of the trains is required to prevent potential failures [4]. Aerodynamic drag, flow around the train, aerodynamic noise, and vibration in extremely unsteady conditions are all common in high-speed trains. It is especially significant when there is a strong crosswind [5].

Crosswinds are caused by wind velocities of varying magnitudes operating in a relative angular direction from the moving train's side. With greater crosswind velocity and lighter material in the next generation high-speed train, the effects of crosswinds on train aerodynamics cannot be avoided. Crosswinds, in principle, could disrupt the vehicle's running stability since aerodynamic forces and moments are magnified. Fig. 1. illustrates component velocity vectors in relation to a moving train subjected to crosswinds (U_w). β is the natural wind direction determined by the train axis, whereas Ψ is the wind direction relative to the train (i.e. the yaw angle), which is a parameter used to address the various crosswind conditions.

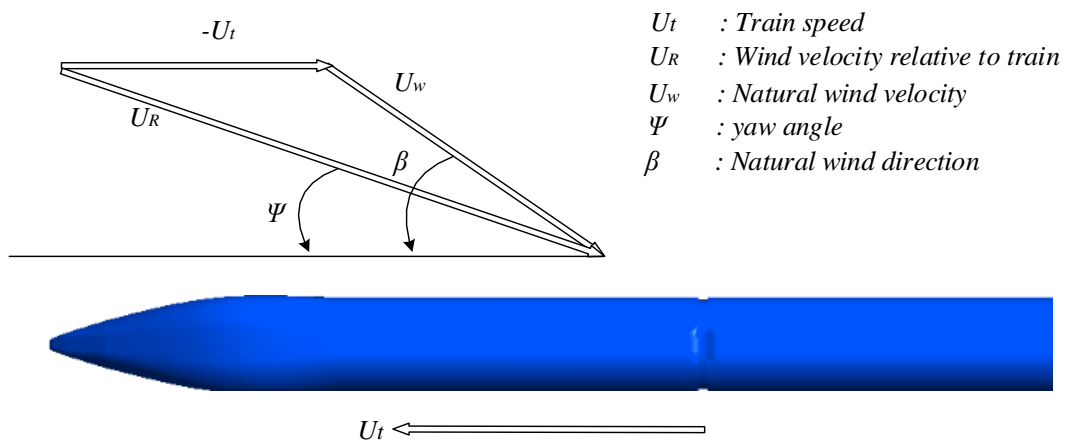


Fig. 1. Natural wind relative to a moving train

Wind criteria, such as natural wind velocity and wind direction, have been determined to be significantly important in evaluating the safety standards of a moving train [6]. In actuality, the wind angle operating on the vehicle in a crosswind is not necessarily constant as it impacts the side of the railway at a yaw angle [7]. This produces forces (aerodynamic loads) that act on the moving train. Aerodynamic loads can have a serious influence on vehicle performance. Crosswind aerodynamic forces provide a crucial wind load that, in extreme situations, can overturn a vehicle. Furthermore, crosswinds can have an impact on the train's running stability and reducing passenger comfort [8].

There are several techniques available for understanding the aerodynamic performance of a high-speed train, including full-scale experiments, computational approaches using computers, and physical modeling. Each method has advantages and disadvantages. In specific, the Computational Fluid Dynamics (CFD) technique has gained popularity in recent years due to its ability to calculate full fluid flow around the train, velocities, and pressures. Despite shortcomings in modeling the transient crosswind condition of train, it is anticipated that CFD capabilities will reach a level of reliability sufficient to eliminate the need for physical model tests in many areas. There are currently a number of suitable modeling approaches available, including steady and unsteady Reynolds-Averaged Navier–Stokes (RANS) techniques, Large Eddy Simulation (LES), and Detached Eddy Simulation (DES). RANS models are widely used in train aerodynamics to study a variety of problems, but they are unable to calculate where there is a very large unsteady condition [9]. The flow patterns

in large-scale separated flows, in particular, will be time-averaged patterns that do not fully represent the conditions found at full scale. However, due to its simplicity and low computational cost, this method has become popular in recent years for solving train aerodynamics problems [10].

In this study, a simplified model of the high-speed concept train Next-Generation Train (NGT) of the German Aerospace Center (DLR) is shown in Fig. 2. The train's three distinguishing features are that it is a very high-speed train running at a maximum of 400 km/hours, with a double-deck configuration and a lightweight design. Nonetheless, this train concept has been proposed because it achieves goals such as low energy consumption and low life-cycle costs per passenger, even with shorter travel times.



Fig. 2 The Next Generation Train (NGT)

Kin *et al.*, [11] have conducted an experiment with straight and side flow over a simplified model of the DLR Next Generation High-Speed Train. The flow fields and aerodynamic forces predicted using these two distinct approaches are compared for the validation instances of the flow through a sphere and the flow around the generic train model. They were primarily concerned with the two prediction methods, so the realistic train model was absent. Furthermore, it does not include the specifics of the acting force coefficients. In the study by Fragner *et al.*, [12], they considered a train model of NGT with a front car and a partial section of the middle car, which is not realistic. They investigated the train's side-wind stability using a different numerical technique. Furthermore, they confirmed the formation of a large vortex system on the train's leeward side, which primarily drives the train's overturning force and moment.

From the standpoint of simulation, the cross-wind stability of a new high-speed train is already taken into account in the early design phase through the use of computational fluid dynamics (CFD). Schiffer and Wagner [13] performed Large Eddy Simulations (LES) of the flow around a simplified concept high-speed train model. Based on the free stream velocity and train width, simulations were run for a Reynolds number of 2×10^5 . The simulations predicted that the laminar flow near the train's nose would transition to a fully turbulent flow in the wake region. The numerical analysis was restricted to the train's nose. As can be seen, very little research has been conducted on the mentioned train, which is being developed by DLR. A comprehensive study is required, which will include both a detailed flow field around the train body in crosswinds. Thus, the overall aim of the study is to investigate the flow structure around a next-generation train subjected to strong crosswind conditions using CFD analysis. The numerical study was carried out using URANS on a simplified NGT model with three coaches (front, middle, and rear) in order to compare it to the original version of the train.

2. Methodology

2.1 3D Model of Next Generation Train

A 1/25th scale model of Next Generation High-Speed Train (NG-HST) was used in the simulations. The original train model was designed by the German Aerospace Centre (DLR) [14]. The model dimensions are shown in Fig. 3. SolidWorks software was used to create the train model. The original front, middle, and rear dimensions of the car are 21m, 20m, and 21m, respectively [15]. As previously

stated, this study used a simplified model; as a result, the 3d model of the NGT maintained the overall size of the original train. However, the train's details have been ignored. In the current study, a 1/25th scale model and three cars (front, middle, and rear) were used to reduce computation costs and achieve optimal simulation performance. This scale model is commonly used in physical scale model testing and CFD simulation. A number of previous researches used this scale model to minimize the computational resource [16-18].

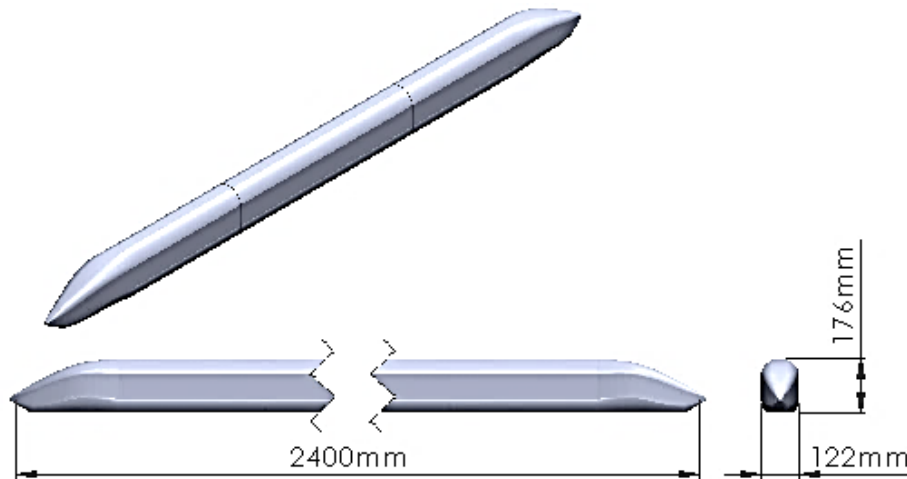


Fig. 3. Simplified next generation train model (1/25th scale)

2.2 Simulation Setup and Boundary Conditions

The computational investigations on the train aerodynamics have been performed using ANSYS FLUENT 2019 software, which is based on a finite volume scheme, and have been performed by solving the governing equations of fluid. In this study, the SIMPLE algorithm is used for pressure–velocity coupling in a pressure-based solver with second-order equations, which makes equation convergence difficult but increases solution precision. The $k-\omega$ SST turbulence model and scalable wall function are used. The $k-\omega$ SST turbulence model predicts flow separation better and can solve turbulence parameters near the wall region [19]. Furthermore, transient simulation mode with 0.02 time steps was used to understand time-dependent flow physics around the train. Each simulation lasts 4 seconds. The non-slip condition is employed with a moving wall boundary condition at the equal speed of the wind with train for the floor surface because this model has a consistent velocity profile and a realistic simulation of the floor. As the symmetry boundary condition, the roof of the enclosure is specified.

Fig. 4 illustrates the computational domain dimensions used in the simulations where L is equal to the length of the train. Previously published works used a variety of enclosure sizes. It is well understood that there are no specific rules for determining enclosure size. However, the enclosure must be large enough to capture the flow field around the train. In the current study, we consider [20] for determining the computational domain size. Thus, the distance from the front boundary to the front nose was 1L, while the distance from the end nose to the end boundary was 2L. The distance from the boundary was 1L measured from the train's left and right sides. The height of rail tracks was represented by the distance between the train wheel and the floor of 0.076L. Furthermore, the train height is considered as the characteristic length. Thus, the Reynolds number was 1.3×10^6 . During simulation, the train speed was 97.22 m/s, while the inlet velocity, which is considered crosswind velocity, was 20 m/s. The pressure outlet was set to zero, referring to atmospheric pressure.

Furthermore, the speed of the train is considered as incompressible flow as the Mach number is less than 0.3 which is 0.28.

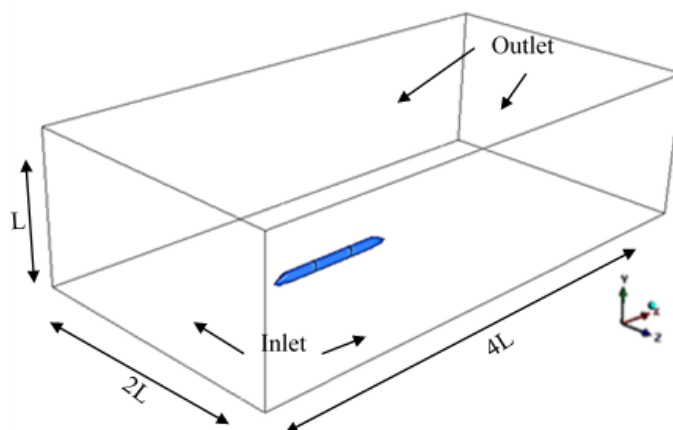


Fig. 4. Boundary conditions used in the simulations

3. Grid Independence Study

In this study, an advanced meshing option in ANSYS FLUENT is used to generate different types of grids with different mesh numbers and mesh quality. Coarse, medium, and fine meshes are generated by varying the number of mesh cells, incorporating a multi-zone meshing technique, and adjusting other mesh refinement options (refer to Table 1). In the computational domain, a cut cells approach is used to generate a structured mesh. It is found that structural mesh provides better results [21]. On the surface of the model train, a 5 layer inflation of prism mesh was introduced to enhance better convergence. Furthermore, the mesh elements are hexahedral, polyhedral, and wedge in shape.

Table 1
 Meshing parameters descriptions

Quality	Coarse	Medium	Fine
Maximum cell size	256 mm	256 mm	128 mm
Total cell number	329,737	665,740	1,206,633
Inflation layer	5	5	5
Growth rate	1.2	1.2	1.15
Refinement box 1	n/a	15mm	10 mm
Refinement box 2	n/a	n/a	20 mm

The coarse meshing had a growth rate of 1.2 with a total of 5 layers. There was no refinement box used in this case. The refinement box used was very close to the train model, which had elements that were 15mm in size. Aside from that, the meshing parameters remain unchanged. The drag coefficient values are influenced by the performance of medium meshing quality.

Fig. 5 illustrates the detail fine meshing with a two refinement box surrounding the train model. Normally, the mesh refinement near the train regions provides better results [22]. The elements in the first refinement box were 10mm in size, while the elements in the second were 20mm in size. Mesh refinement in Fig. 5(a) yields good results in terms of mesh quality between car gaps. In addition to the previous meshing, a 5 layer inflation layer was added (Fig. 5(b)). However, the growth rate was

reduced to 1.15 percent. Fig. 5 (c) demonstrates a high-quality mesh at the train's nose. The average y -plus value on the train surface was 48, which is within the acceptable range as stated in previous literature [23].

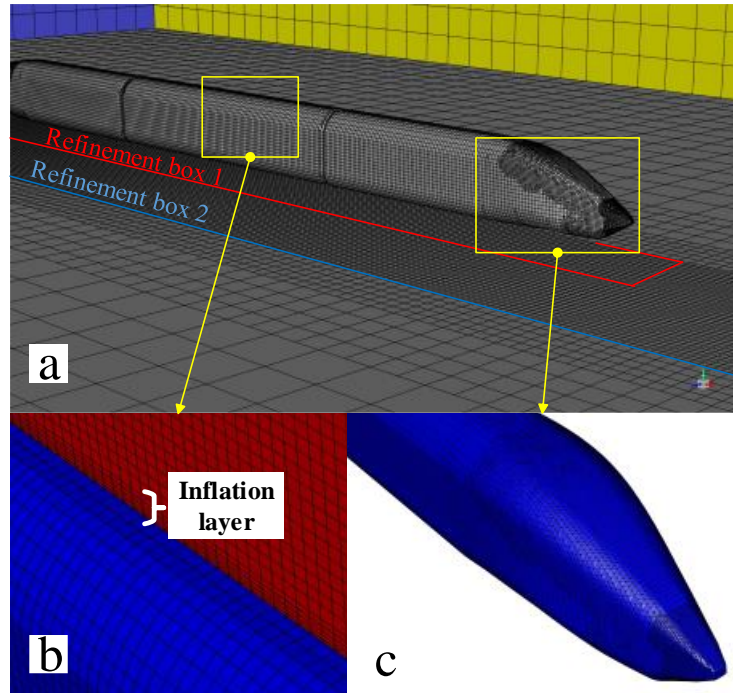


Fig. 5. Details of fine mesh; (a) train body surface, (b) inflation layers in the middle car's surface, and (c) end car nose

The experimental data from the wind tunnel for this model train is not available in the literature. As a result, the authors look for cases that are similar to validate the simulation results. The authors are aware that, even though it will not reflect the exact results, it will contribute to the validation of the current study's model. The current study was validated using the experimental results of Sun *et al.*, [24]. Table 2 shows that the simulation result is primarily in good agreement with the experimental results. The maximum relative error was 5.4%.

Table 2
 Comparison between simulation and experimental result by Sun *et al.*, [24]

Condition	C_d				Relative error (%)
	Head	Middle	Tail	Total	
Coarse	0.1054	0.0955	0.1502	0.3512	1.007
Medium	0.0989	0.0939	0.1438	0.3367	3.164
Fine	0.0957	0.0938	0.1393	0.3289	5.407
Experiment by Sun <i>et al.</i> , (2021)	0.1346	0.0808	0.1323	0.3477	

4. Results

4.1 Surface Streamlines

The flow pattern on the train's surface is performed by surface streamlines at crosswind angles of 5°, 10°, 15°, and 20°. Fig. 6 shows how the flow starts to separate from the nose of the first coach to the end nose of the train. As the train approaches to expose in 5° to 10° crosswind angles, a larger separation angle appears on the top of the train, demonstrating that three-dimensional features

describe the flow around the train. This is mostly due to a result of natural and train-induced wind on the train's nose area. Specifically, as crosswind angles increased, flow separation increased significantly as shown in Fig. 6(c). Furthermore, flow separation on the leeward side is slightly different when the train is exposed to a 15° yaw angle. The flow that separates from the windward roof top corner is redirected at an angle along the train axis as it passes over the train head. It can be concluded that a larger yaw angle, which is mostly determined by the incoming wind velocity, can lead to higher flow separation and a more complicated three-dimensional flow around the train [25]. Fig. 6(d) shows the evidence of higher flow separation at larger yaw angles.

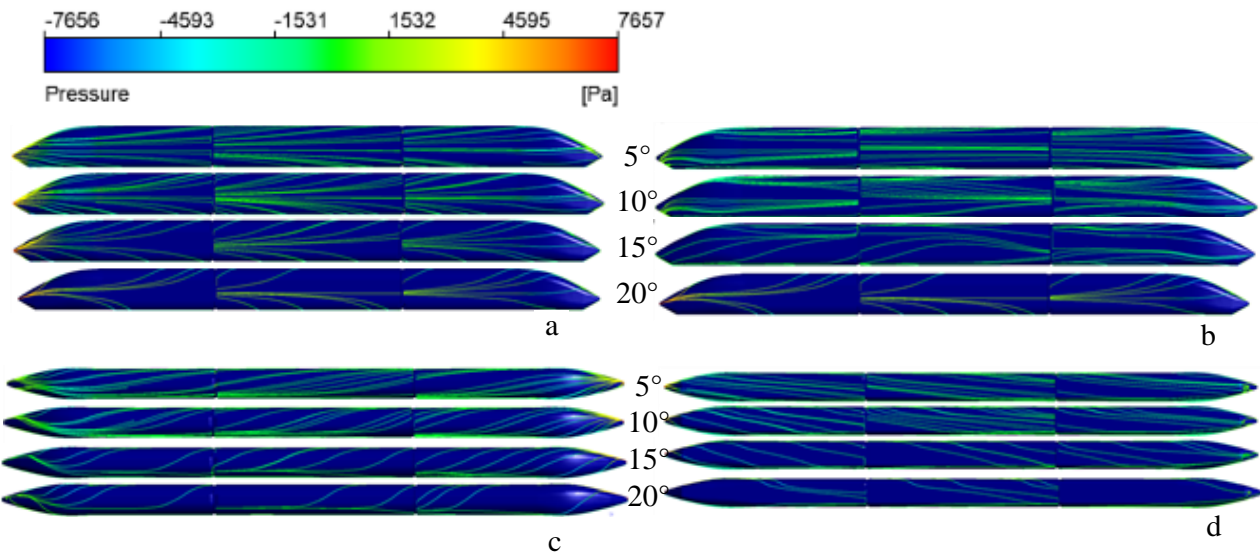


Fig. 6. Surface streamlines on train surface; (a) windward, (b) leeward, (c) roof top and (d) underbody

4.2 Iso-surface of the Instantaneous Velocity

Fig. 7 depicts the vortex formed on the train's leeward side. Following vortex generated on the train from different areas:

- V1: vortex origin from the front bottom leeward side of the front car
- V2: vortex origin from the front top leeward side of the front car
- V3: vortex origin from the front center side of the middle car
- V4: vortex origin from the rear top side of the middle car

At a 5° yaw angle, a small vortex denoted by V1 formed on the leeward side, which began to develop from the middle car and began to dissipate at the tail of the train as shown in Fig. 7(a). Furthermore, V2 formed at the nose of front car and disappeared very soon. Fig. 7(b) shows two large vortices V1 and V2 for a yaw angle of 10°. The vortex began to separate from the end of the first coach and continued until the tail and beyond. Furthermore, those two vortices formed, one from the upper part of the leeward side and another from the bottom part, indicating that the vortices formed as a result of the flow passed over the roof top and underbody, respectively.

At the 15° yaw angle condition, a number of vortex can be observed. Among them, V1, formed from the rear bottom side of front car and continued parallel with the train. Same goes for the vortex V2, however, which is started left top edge of front car. Interestingly vortex V3 formed near front nose and bottom edge of leeward side and move further and go away from the train model in the leeward-rear direction (see Fig. 7(c)).

V1 developed from the lower-left edge of the front car and continued to move further until front of the middle car of the train shown in Fig. 7(d). V2 is a vortex formed by the left upper side of the front car. V3 vortex formed near the bottom of the leeward side and moved away from the train model in the leeward-rear direction. Vortex V4 evolved from the rear end of the middle car and was combined with a tailing vortex. A comparison of flow streamlines at different wind angles demonstrates that when the wind angle is low, the separation of flow and wakes is limited to the end of the train. However, when the wind angle increases, flow separation develops from the top and lower corners of the train and similar results reported by Ezoji *et al.*, [26]. In addition, a number of tailing vortices can be seen in all the different yaw angles. It is understandable from Fig. 7(c) and Fig. 6 that the flow separation is large when the train is exposed to larger yaw angles. As a result, it is demonstrated that surface streamlines produce similar results in this regard.

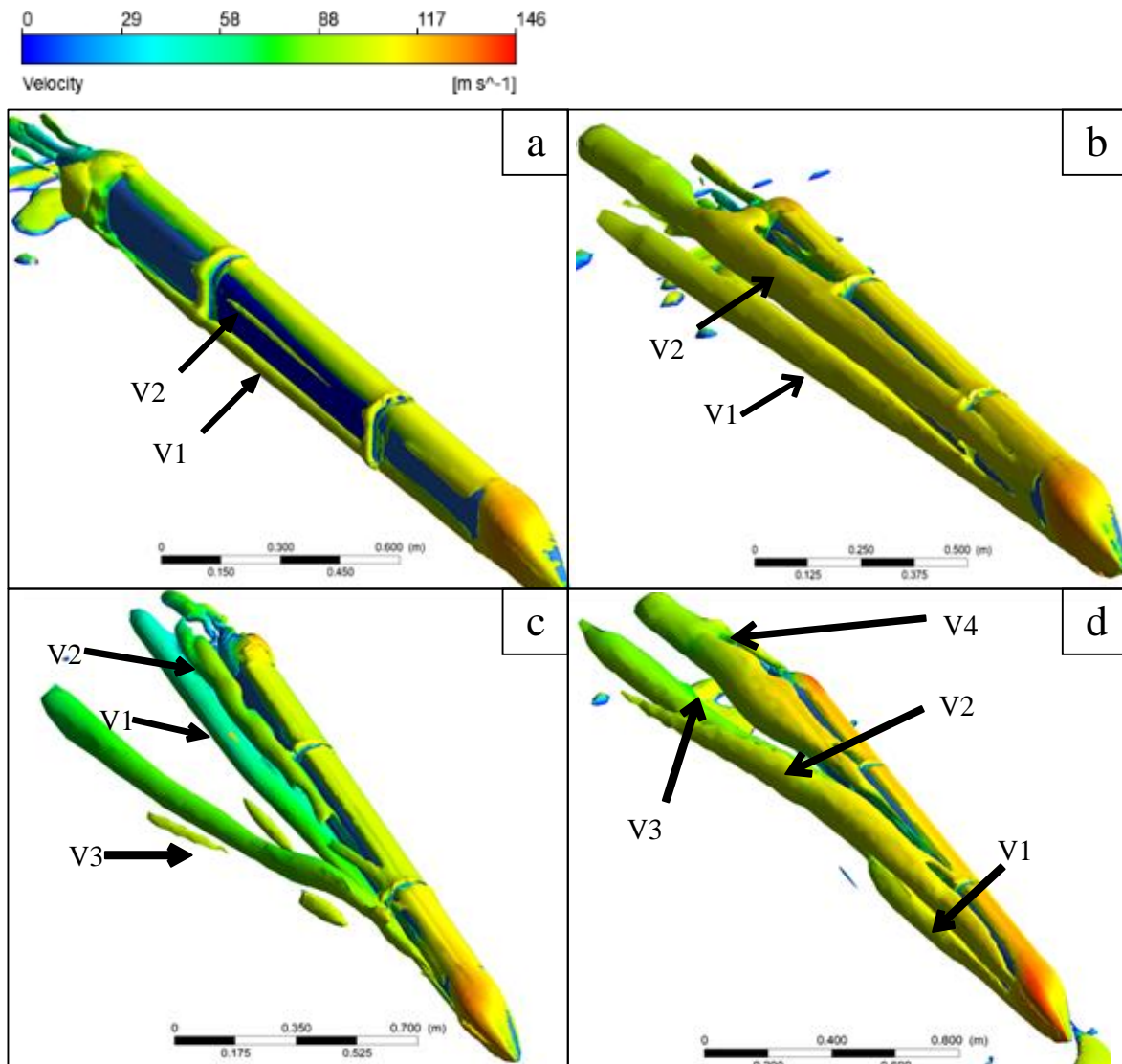


Fig. 7. Iso-surface of velocity for different yaw angles; (a) 5°, (b) 10°, (c) 15°, and (d) 20°

4.3 Pressure Coefficient

The aerodynamic force is calculated by integrating the surface pressure coefficient, which has a direct influence on the train's aerodynamic forces. The non-dimensional pressure value is presented

along with the train's centerline in Fig. 8. Because of the stagnation pressure, there is a substantial increase in static pressure on the train's nose, followed by a significant drop surrounding the nose when the velocity of air increases in this location. With the exception of the car gaps, when static pressure increases, the pressure along the train length and within the slip-stream boundary layer is typically slightly lower than the upstream pressure. There is also a drop in static pressure at the train's tail. Pressure rises in the circulation region behind the train, while pressure increases in the near wake region. As the yaw angle increases, so the negative pressure is increased [27]. It can be seen that the pressure curves for the 10° and 15° yaw angles are nearly identical. The curve for the 20° yaw angle, on the other hand, is slightly different. This could be the cause of the increasing complexity in flow separation seen in Fig. 7(d). On the other hand, the situation can be described for the 5° yaw angle, where the pressure coefficient value is slightly higher than others, possibly due to the simplicity of the flow around the train.

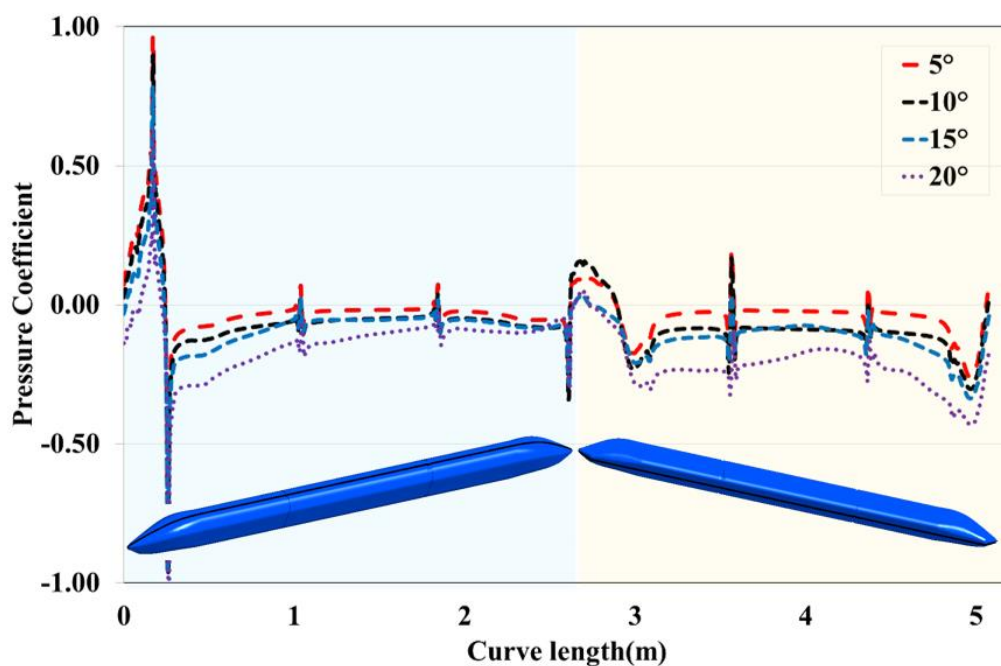


Fig. 8. Pressure coefficient along with the curve length of train in different yaw angles

5. Conclusions

CFD analysis was used in this study to investigate the flow structure around a Next-Generation Train in the presence of a strong crosswind at low yaw angles. This is one of the first studies in which a full train model, including the front, middle, and rear cars of a next-generation train, is used for CFD analysis. For various yaw angles, time-average surface streamlines, the iso-surface of the instantaneous velocity, and the pressure coefficient are presented.

A larger yaw angle, which is primarily determined by the incoming wind velocity, can lead to higher flow separation and a more complex three-dimensional flow around the train. On the other hand, a comparison of iso-surface and flow streamlines at different wind angles reveals that when the wind angle is small, separation of flow and wakes is limited to the end of the train, but as the wind angle increases, separation of flow occurs from the upper and bottom corners of the train, indicating that the vortices formed as a result of the flow passing over the roof top and underbody. In addition, at 20° yaw angle, the pressure coefficient curve is slightly different than others. This could be the cause of the increasing complexity in flow separation caused by the large wind angle.

Acknowledgement

This research was financially supported by the Malaysia Ministry of Higher Education (MOHE) through Fundamental Research Grant Scheme (FRGS/1/2020/TK02/UTHM/03/4).

References

- [1] Lee, Woo Geun, Jung-Seok Kim, Seung-Ju Sun, and Jae-Yong Lim. "The next generation material for lightweight railway car body structures: Magnesium alloys." *Proceedings of the Institution of Mechanical Engineers, Part F: Journal of Rail and Rapid Transit* 232, no. 1 (2018): 25-42. <https://doi.org/10.1177/0954409716646140>
- [2] Rochard, B. P., and Felix Schmid. "Benefits of lower-mass trains for high speed rail operations." In *Proceedings of the Institution of Civil Engineers-Transport*, vol. 157, no. 1, pp. 51-64. Thomas Telford Ltd, 2004. <https://doi.org/10.1680/tran.2004.157.1.51>
- [3] Lei, Y. Lightweight Design of High-speed Train under the Development of New Materials. In *Proceedings of 5th International Conference on Vehicle, Mechanical and Electrical Engineering* (2019): 217–221. SCITEPRESS - Science and Technology Publications. <https://doi.org/10.5220/0008865102170221>
- [4] Dillmann, Andreas, Gerd Heller, Ewald Krämer, Claus Wagner, and Christian Breitsamter, eds. *New results in numerical and experimental fluid mechanics X: Contributions to the 19th STAB/DGLR Symposium Munich, Germany, 2014*. Vol. 132. Springer, 2016.
- [5] Gallagher, Martin, Justin Morden, Christopher Baker, David Soper, Andrew Quinn, Hassan Hemida, and Mark Sterling. "Trains in crosswinds—comparison of full-scale on-train measurements, physical model tests and CFD calculations." *Journal of Wind Engineering and Industrial Aerodynamics* 175 (2018): 428-444. <https://doi.org/10.1016/j.jweia.2018.03.002>
- [6] Imai, Toshiaki, Toshishige Fujii, Katsuji Tanemoto, Taisuke Shimamura, Tatsuo Maeda, Hiroaki Ishida, and Yu Hibino. "New train regulation method based on wind direction and velocity of natural wind against strong winds." *Journal of wind engineering and industrial aerodynamics* 90, no. 12-15 (2002): 1601-1610. [https://doi.org/10.1016/S0167-6105\(02\)00273-8](https://doi.org/10.1016/S0167-6105(02)00273-8)
- [7] Suzuki, Minoru, Katsuji Tanemoto, and Tatsuo Maeda. "Aerodynamic characteristics of train/vehicles under cross winds." *Journal of wind engineering and industrial aerodynamics* 91, no. 1-2 (2003): 209-218. [https://doi.org/10.1016/S0167-6105\(02\)00346-X](https://doi.org/10.1016/S0167-6105(02)00346-X)
- [8] Cui, Tao, Weihua Zhang, and Bangcheng Sun. "Investigation of train safety domain in cross wind in respect of attitude change." *Journal of Wind Engineering and Industrial Aerodynamics* 130 (2014): 75-87. <https://doi.org/10.1016/j.jweia.2014.04.006>
- [9] Cheng, H., L. J. Zhou, and Y. Z. Zhao. "Very large eddy simulation of swirling flow in the Dellenback abrupt expansion tube." In *IOP Conference Series: Earth and Environmental Science*, vol. 163, no. 1, p. 012084. IOP Publishing, 2018. <https://doi.org/10.1088/1755-1315/163/1/012084>
- [10] Kamal, Muhammad Nabil Farhan, Izuan Amin Ishak, Nofrizalidris Darlis, Daniel Syafiq Baharol Maji, Safra Liyana Sukiman, Razlin Abd Rashid, and Muhamad Asri Azizul. "A Review of Aerodynamics Influence on Various Car Model Geometry through CFD Techniques." *Journal of Advanced Research in Fluid Mechanics and Thermal Sciences* 88, no. 1 (2021): 109-125. <https://doi.org/10.37934/arfmts.88.1.109125>
- [11] Kin, Natalia, Ralf Deiterding, and Claus Wagner. "Large Eddy Simulations of Side Flow Past a Generic Model of a High-Speed Train." In *New Results in Numerical and Experimental Fluid Mechanics X*, pp. 421-431. Springer, Cham, 2016. https://doi.org/10.1007/978-3-319-27279-5_37
- [12] Fagner, Moritz M., and Ralf Deiterding. "Investigating side-wind stability of high speed trains using high resolution large eddy simulations and hybrid models." In *European Congress on Computational Methods in Applied Sciences and Engineering*, pp. 223-241. Springer, Cham, 2015. https://doi.org/10.1007/978-3-319-54490-8_14
- [13] Schiffer, Stefanie, and Claus Wagner. "Numerical Investigation of Time-Dependent Cross-Wind Effects on an Idealised Leading Rail Car." (2012). *Civil-Comp Proceedings*, 98. <https://doi.org/10.4203/ccp.98.164>
- [14] Siefkes, T. (2012). Next Generation Train. Retrieved December 16, 2021, from <https://verkehrsforschung.dlr.de/en/projects/ngt-hst>
- [15] Winter, Joachim. "Novel rail vehicle concepts for a high speed train: the next generation train." In *Proceedings of the First International Conference on Railway Technology: Research, Development, Maintenance*. Civil-Comp Press, 2012. <http://dx.doi.org/10.4203/ccp.98.22>
- [16] Hashmi, Syeda Anam, Hassan Hemida, and David Soper. "Wind tunnel testing on a train model subjected to crosswinds with different windbreak walls." *Journal of Wind Engineering and Industrial Aerodynamics* 195 (2019): 104013. <http://doi.org/10.1016/j.jweia.2019.104013>

- [17] Heckmann, Andreas, Bernhard Kurzeck, Tilman Bunte, and Sigfried Loose. "Considerations on active control of crosswind stability of railway vehicles." *Vehicle System Dynamics* 52, no. 6 (2014): 759-775. <https://doi.org/10.1080/00423114.2014.901539>
- [18] Dorigatti, F., M. Sterling, C. J. Baker, and A. D. Quinn. "Crosswind effects on the stability of a model passenger train—A comparison of static and moving experiments." *Journal of Wind Engineering and Industrial Aerodynamics* 138 (2015): 36-51. <http://dx.doi.org/10.1016/j.jweia.2014.11.009>
- [19] Menter, F. R., R. Lechner, and A. Matyushenko. "Best practice: generalized k- ω two-equation turbulence model in ANSYS CFD (GEKO)." *Technical Report, ANSYS* (2019): 27.
- [20] Wang, Shuangbu, Ruibin Wang, Yu Xia, Zhenye Sun, Lihua You, and Jianjun Zhang. "Multi-objective aerodynamic optimization of high-speed train heads based on the PDE parametric modeling." *Structural and Multidisciplinary Optimization* (2021): 1-20. <https://doi.org/10.1007/s00158-021-02916-0>
- [21] Abobaker, Mostafa, Sogair Addeep, Lukmon O. Afolabi, and Abdulhafid M. Elfaghi. "Effect of Mesh Type on Numerical Computation of Aerodynamic Coefficients of NACA 0012 Airfoil." *Journal of Advanced Research in Fluid Mechanics and Thermal Sciences* 87, no. 3 (2021): 31-39. <https://doi.org/10.37934/arfmts.87.3.3139>
- [22] Ahmad, Nor Elyana, Essam Abo-Serie, and Adrian Gaylard. "Mesh optimization for ground vehicle aerodynamics." *CFD Letters* 2, no. 1 (2010): 54-65.
- [23] Ishak, I. A., M. S. M. Ali, and SAZ Shaikh Salim. "Numerical simulation of flow around a simplified high-speed train model using OpenFOAM." In *IOP Conference Series: Materials Science and Engineering*, vol. 152, no. 1, p. 012047. IOP Publishing, 2016. <http://doi.org/10.1088/1757-899X/152/1/012047>
- [24] Sun, Zhenxu, Shuanbao Yao, Lianyi Wei, Yongfang Yao, and Guowei Yang. "Numerical Investigation on the Influence of the Streamlined Structures of the High-Speed Train's Nose on Aerodynamic Performances." *Applied Sciences* 11, no. 2 (2021): 784. <https://doi.org/10.3390/app11020784>
- [25] Yao, Zhiyong, Nan Zhang, Xinzhong Chen, Cheng Zhang, He Xia, and Xiaozhen Li. "The effect of moving train on the aerodynamic performances of train-bridge system with a crosswind." *Engineering Applications of Computational Fluid Mechanics* 14, no. 1 (2020): 222-235. <https://doi.org/10.1080/19942060.2019.1704886>
- [26] Ezoji, Reza, and Mohammad Reza Talaei. "Analysis of Overturn of High-Speed Train with Various Nose Shapes Under Crosswind." *Iranian Journal of Science and Technology, Transactions of Mechanical Engineering* (2021): 1-14. <https://doi.org/10.1007/s40997-021-00426-4>
- [27] Niu, Jiqiang, Xifeng Liang, and Dan Zhou. "Experimental study on the effect of Reynolds number on aerodynamic performance of high-speed train with and without yaw angle." *Journal of Wind Engineering and Industrial Aerodynamics* 157 (2016): 36-46. <http://dx.doi.org/10.1016/j.jweia.2016.08.007>